Design and Energetic Characterization of a Proportional-Injector Monopropellant-Powered Actuator

Kevin B. Fite, *Member, IEEE*, and Michael Goldfarb, *Member, IEEE*

***Abstract*—This paper describes the design and energetic characterization of an actuator designed to provide enhanced system energy and power density for self-powered robots. The proposed actuator is similar to a typical compressible gas fluid-powered actuator, but pressurizes the respective cylinder chambers via a pair of proportional injector valves, which control the flow of a liquid monopropellant through a pair of catalyst packs and into the respective sides of the double-acting cylinder. This paper describes the design of the proportional injection valves and describes the structure of a force controller for the actuator. Finally, an energetic characterization of the actuator shows improvement relative to prior configurations and marked improvement relative to state-of-the-art batteries and motors.**

***Index Terms*—Energetic characterization, monopropellant-powered actuation, power-autonomous robots.**

I. Introduction

ENERGETIC deficiencies in current power supply and actuation technology limit significantly the utility of human-scale self-powered robots (see, for example, discussion in [1]). Such deficiencies have motivated the development of alternative actuators that have the potential to deliver improved energetic characteristics relative to battery-powered servomotors. Goldfarb *et al*. and Shields *et al*. describe two types of liquid-monopropellant-powered actuators, a centralized and a direct-injection type, respectively, that provide improved energetic properties relative to battery-powered servomotors [1]–[3]. Although monopropellants have been used in thrusters in numerous aerospace applications (see, for example, [4]–[6]), and recently as the power source for a free piston hydraulic pump [7], little prior work exists regarding their use in servo-controlled actuators. The first appearance of such work, described by Goldfarb *et al*. [1], is much like a standard pneumatic actuation system, but utilizes a monopropellant gas generator in place of an air compressor. The configuration described in [1] incorporates a solenoid valve to meter the flow of hydrogen peroxide through a catalyst pack and into a high-pressure hot gas reservoir. Like a conventional pneumatic actuation system, a four-way proportional spool valve controls the flow of compressible fluid (in this case a hot gas) from the reservoir into one side of a pneumatic piston, while exhausting the other side to atmosphere. The servocontrol of this system is therefore nearly identical to a standard pneumatic servosystem, and as such, a standard control approach was used (i.e., a full-state-feedback position-velocity-acceleration controller). As in most fluid-powered actuators, high-bandwidth control of power is achieved via dissipative means (i.e., the gas flow is throttled via a servovalve), which can significantly decrease the efficiency of energy conversion. Rather than using a servovalve to modulate a high-power gas flow, the configuration described by Shields *et al*. [2] uses solenoid valves to modulate the (low power) flow of liquid propellant, and thus essentially eliminates power losses due to fluid throttling (i.e., the fuel flow rates are orders of magnitude lower than the gas flow rates, and as such, control losses are essentially eliminated). In the configuration described in [2] and [3], the pressurized propellant is injected via solenoid injection valves through catalyst packs directly into the respective sides of a pneumatic cylinder, and thus the configuration is termed solenoid-injector direct-injection (SIDI). The cylinder chambers are depressurized via a proportional three-way spool valve, which can exhaust one cylinder chamber or the other at any given time. The centralized configuration described in [1] provided an energetic figure of merit (as subsequently described herein) approximately three times better than state-of-the-art batteries and motors, while the same energetic figure of merit for the SIDI configuration was approximately ten times better than state-of-the-art batteries and motors [2], [3]. The improvement between the centralized and SIDI system was due to a combination of improved efficiency of conversion and improved power density. The direct-injection configuration utilized solenoid (i.e., binary on/off) valves to control the flow rate of propellant through the catalyst packs, since proportional injection valves with the requisite size and flow rate characteristics were commercially not available. Use of solenoid rather than proportional injector valves entails a substantial tradeoff between flow rate resolution and maximum flow rate. Flow rate resolution is a function of the orifice size and the minimum opening time, while maximum flow rate is solely a function of the orifice size. Given a certain minimum opening time (1 ms for the valves used in [2] and [3]), a smaller orifice size limits the maximum flow rate (i.e., maximum actuator power), while a larger size limits resolution (i.e., force tracking resolution). In the case of the solenoid-injected system described in [2] and [3], the valve characteristics were chosen to provide a desired level of resolution, and as such the

Manuscript received September 15, 2005; revised November 30, 2005. Recommended by Guest Editors S. Agrawal and V. Krovi. This work was supported in part by Defense Advanced Research Projects Agency (DARPA) under Grant DAAD190110509 and by the National Science Foundation (NSF) under Grant IIS0307651.

The authors are with the Department of Mechanical Engineering, Vanderbilt University, Nashville, TN 37235 USA (e-mail: kevin.fite@vanderbilt.edu; michael.goldfarb@vanderbilt.edu).

Digital Object Identifier 10.1109/TMECH.2006.871097

Fig. 1. Prototype proportional liquid fuel valve (shown in box), with the catalyst pack attached at the output.

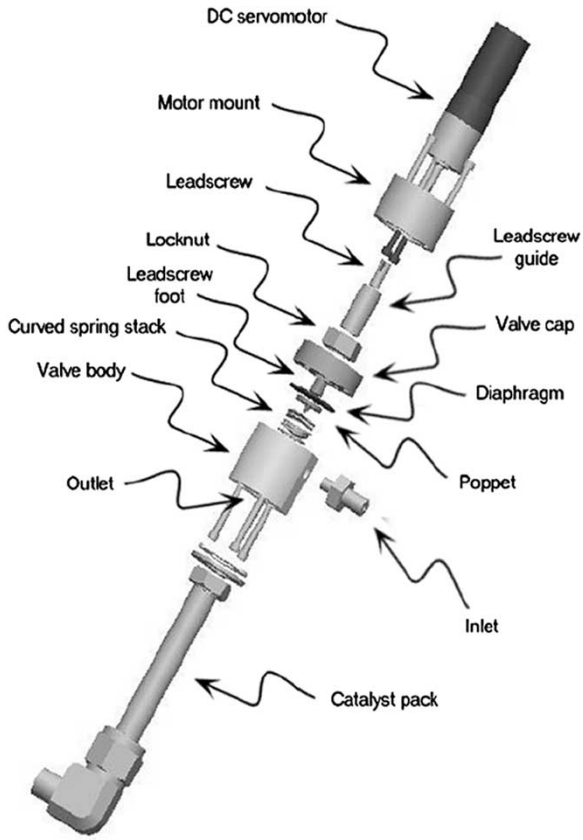

Fig. 2. Exploded view of the proportional valve and catalyst pack.

maximum power, and thus the actuator power density, was compromised. In order to circumvent the power/resolution tradeoff in the direct-injection system, the authors developed proportional injection valves for use in a proportional-injector direct-injection (PIDI) configuration. This paper describes the resulting system, and in particular 1) describes the design of the injection valves, 2) describes the force controller utilized for the energetic characterization, and 3) presents experimental results that characterize the energetic performance of the actuation system.

II. Proportional Injection Valve Design

On the basis of the experimental data of the flow requirements for the solenoid injection system described in [2] and [3], it may be infered that the proportional injection valves must operate at pressures of 2.0 MPa (300 psi) and must provide high-resolution high-bandwidth flow control up to maximum flow rates on the order of 1 mL/s. Additionally, in order to minimize the transport delay in the dynamics of propellant decomposition, the dead volume between the injection valve orifice and the catalyst pack should be minimized. Finally, since the catalyst pack reaches temperatures of 232 °C (450 °F), the injection valve sensing and actuation must be thermally isolated from the catalyst pack.

Since no liquid valve with the desired characteristics is commercially available, custom valves were designed and fabricated for use in the proportional-injection actuator prototype. Fig. 1 shows a prototype injection valve, with a catalyst pack attached at its output. The valve is a hybrid poppet-needle-diaphragm type, since it utilizes design concepts from all of these common valve configurations in order to obtain a compact proportional valve that can deliver the desired flow resolution with a closed-loop bandwidth of the order of 10 Hz. Fig. 2 shows an exploded view of the valve/catalyst pack system. The valve is a direct-acting type, where valve actuation is accomplished via a dc servomotor with integrated encoder and gearhead, chosen for its compact package and ease of control. The servomotor package actuates a tapered poppet assembly through a lead screw and diaphragm. Using a diaphragm (as opposed to a sliding seal) fully isolates the servomotor package from the pressurized fuel without requiring sliding contact, thus minimizing friction and ensuring a seal. The tapered poppet assembly consists of a cylindrical bronze insert, which acts as a rotary bearing that prevents twisting of the diaphragm (i.e., from the lead screw), the tapered poppet, and a stack of curved spring washers that facilitate the return of the poppet assembly. Using a tapered (as opposed to a flat) poppet enables higher resolution in flow control. The minimum orifice area exposed to flow is defined by the minimum annulus between the diameter of the valve orifice and the largest diameter of the tapered cone that remains within the orifice. The sensitivity of annular area to lead screw travel can therefore be adjusted by varying the included angle of the taper. A decreased included angle of the taper results in increased flow rate resolution, but decreases control bandwidth (due to increased lead screw travel). Experimental trials converged on a tapered poppet with an included angle of 20° for an orifice diameter of 1.3 mm (0.052 in), which requires a total poppet travel of 0.65 mm (0.025 in). This geometry provided a combination of good resolution (especially in the expected operating

regions of lower fluid flow rates) and acceptable bandwidth (i.e., approximately 10 Hz). Note that sealing the valve at the outlet rather than at the inlet, which is enabled by the use of the curved spring washers, is advantageous from the perspective of controlling the liquid-fueled actuator because it minimizes the dead volume through which the fuel must flow before reaching the catalyst pack. Minimizing the dead volume serves to minimize any transport delay associated with fluid flow, which would adversely affect the closed-loop performance of the actuation system. The valve body and tapered poppet are fabricated from polyetherether-ketone (PEEK), which was chosen for its compatibility with hydrogen peroxide (the fuel of interest for the proposed actuator) and its low thermal conductivity (since the motor must be thermally isolated from the catalyst pack). The valve cap is fabricated from bronze, which offers compatibility with hydrogen peroxide (though no contact with hydrogen peroxide is expected under normal operating conditions) and the material strength to hold threads for securing the valve body and the motor mount. The diaphragm consists of a round sheet of Viton elastomer with a thickness of 0.74 mm (0.029 in), sandwiched between the valve body and the cap. The valve body and the cap were designed so that tightening the cap flush with the valve body results in 0.18-mm (0.007 in) compression of the diaphragm, which effectively prevents leakage of both gaseous and liquid working fluids up to the desired operating pressures of 2.0 MPa (300 psi). The dc servomotor package consists of a dc motor with a 43:1 gearhead and an integrated 512-count encoder (MicroMo model 1524SR-16/7-43:1-IE2-512), which provides a rated output torque of 108 $\text{mN} \cdot \text{m}$ (0.95 $\text{in} \cdot \text{lb}$). The catalyst pack consists of a 9.5 mm (0.375 in) diameter stainless steel tube threaded into the outlet port of the valve body. Within the tube, iridium-coated alumina catalyst granules fill the entire inner volume and are held in place by a fine-mesh stainless steel screen at each end. A fitting attached to the end of the catalyst pack provides for coupling the output of the catalyst pack to an inlet port of the hot-gas cylinder. Figs. 3 and 4 show cross-sectional views of the proportional valve in its closed and full-open positions, respectively. In Fig. 3 (the fully closed position), the pressurized liquid occupies the inlet (bottom of the drawing) and surrounds the wave springs and the poppet in the chamber. The liquid is confined in the chamber between the plugged outlet on the left and the diaphragm on the right. In Fig. 4 (the fully open position), the liquid flows into the inlet, through the chamber, out through the outlet port, and finally into the catalyst pack (on the left side of the drawing), which is filled with catalyst material (not shown). The flow characteristics of the valve, measured using water pressurized to 2.0 MPa, are shown in Fig. 5. The valve exhibits a maximum flow rate of 9 mL/s and a closed-loop bandwidth of 10 Hz. The complete power-production package consists of a total length of 18 cm and maximum diameter of 2.5 cm.

III. Force Control

Fig. 6 shows the complete PIDI actuator package, which includes a pair of proportional injection valves (previously described), a single three-way exhaust valve (described in detail

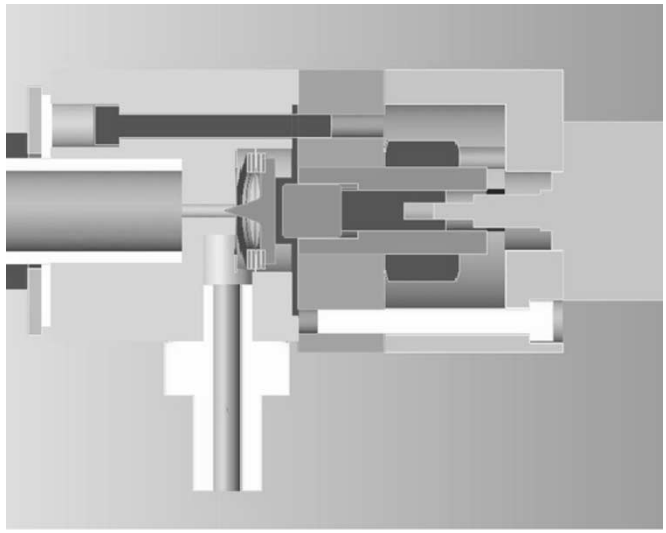

Fig. 3. Cross-sectional view of the closed proportional valve.

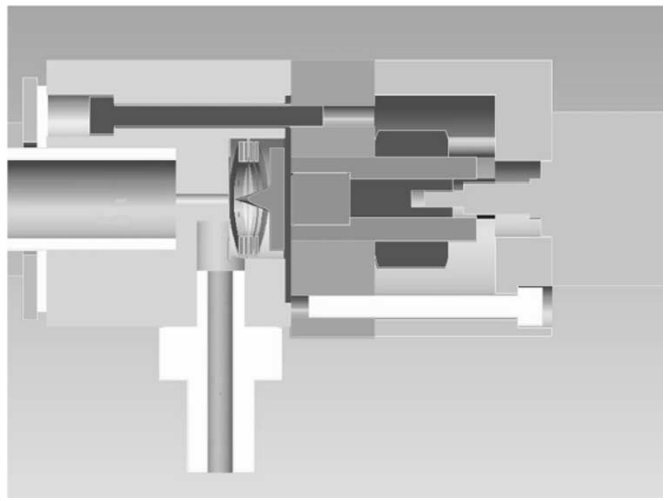

Fig. 4. Cross-sectional view of the full-open proportional valve.

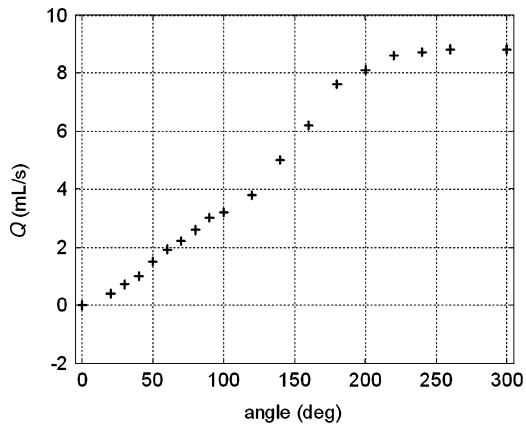

Fig. 5. Volumetric flow rate characteristics of the proportional injection valve. The average flow rate was measured at each point by measuring the amount of time required to fill a given volume in a graduated cylinder.

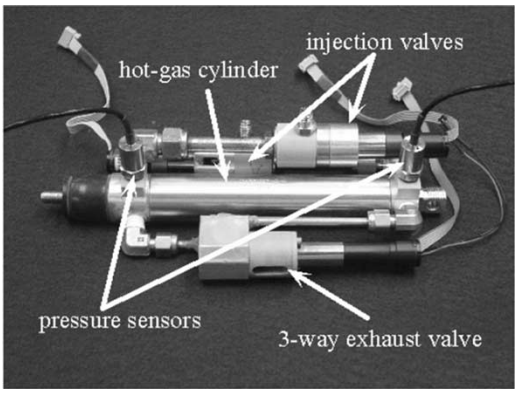

Fig. 6. PIDI actuator package.

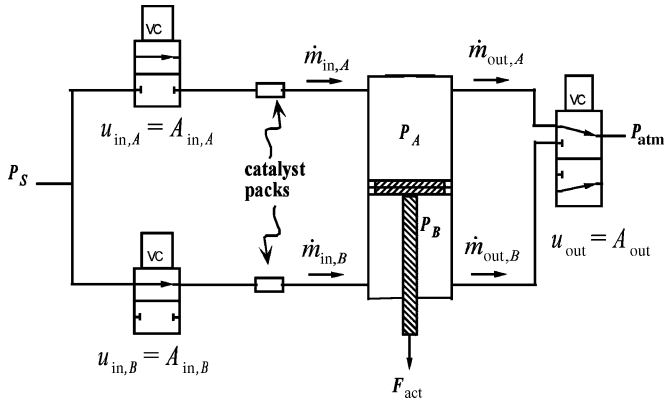

Fig. 7. Schematic of PIDI actuator.

in [8]), a hot-gas cylinder (Bimba model 094-DX), and two pressure sensors (Entran model EPXT), one for each actuator chamber.

Previous work (described in [9]) on the control of the PIDI actuator developed a unified control structure based on a sliding-mode controller for the control of actuator force. Although the unified controller works well (e.g., force tracking bandwidth in excess of 5 Hz), the "black box" nature of the controller does not allow direct control of the individual cylinder pressures. Such control is desirable in order to minimize fuel consumption (see, for example, [10]). Adoption of the unified controller described in [9] would presumably result in better tracking performance, but would preclude direct control of chamber pressures, and thus would increase propellant consumption relative to a direct pressure control approach. Thus, in order to afford enhanced actuator efficiency, an alternative controller was developed that controls directly the pressures in each chamber, then imposes an outer force control loop around these inner pressure control loops. The controller is structured as follows.

For the actuator shown schematically in Fig. 7, the actuator force is given by

$$F = P_A A_A - P_B A_B - P_{\text{atm}} A_r \tag{1}$$

where P_A and P_B are the pressures in the chambers A and B, A_A, and A_B are the cross-sectional areas of chambers A and B, respectively, P_{atm} is the atmospheric pressure, and A_r is the cross-sectional area of the piston rod. The pressure dynamics for a given actuator chamber, assuming an ideal gas undergoing an isothermal process, are given by

$$\dot{P} = \frac{RT}{V}(\dot{m}_{\text{in}} - \dot{m}_{\text{out}}) - \frac{\dot{V}}{V}P \tag{2}$$

where V is the chamber volume, R is the specific gas constant, T is the adiabatic decomposition temperature of the monopropellant, $\dot{m}_{\text{in}}$ is the mass flow rate of the gas entering the actuator chamber, and $\dot{m}_{\text{out}}$ is the mass flow rate of the gas leaving the actuator chamber. The inlet mass flow rate is determined by the monopropellant decomposition dynamics, presented in [9], and can be described by

$$\tau_s \ddot{m}_{\text{in}} + \dot{m}_{\text{in}} = A_{\text{in}} c \sqrt{2\rho_L (P_s - P)} \tag{3}$$

where τ_s is the time constant governing the rate of heat release from the monopropellant decomposition, P_s is the supply pressure in the fuel tank, A_{in} is the orifice area of the proportional liquid valve, c is the discharge coefficient of the injection valve, and ρ_L is the density of the monopropellant. The dynamics governing the mass flow rate of the gas leaving the actuator chamber can be expressed, as presented in [9]

$$\dot{m}_{\text{out}} = \Psi(P) A_{\text{out}} \tag{4}$$

where A_{out} is the orifice area of the exhaust valve and $\Psi(P)$ is an algebraic function of cylinder pressure defined by (5), shown at the bottom of the page, where C_f is the discharge coefficient for the exhaust valve, P is the pressure in the cylinder chamber, P_{atm} is the downstream pressure (atmospheric), C_r is the critical ratio governing the transition between subsonic and sonic flow, and C_1 and C_2 are constants defined by

$$C_1 = \sqrt{\frac{\gamma}{R}\left(\frac{2}{\gamma+1}\right)^{(\gamma+1)/(\gamma-1)}} \tag{6}$$

$$C_2 = \sqrt{\frac{2\gamma}{R(\gamma-1)}} \tag{7}$$

where γ is the ratio of specific heats of the gas.

The controller strategy is to directly control (with injection and exhaust) the pressure of a single chamber while imposing no control effort on the opposing chamber, thereby controlling the output force of the actuator. Exclusive control of a single chamber precludes simultaneous injection and/or exhaust of both chambers and thus lends itself to enhanced efficiency. The sign of the desired actuator force command determines the particular

$$\Psi(P) = \begin{cases} \frac{C_1 C_f P}{\sqrt{T}} & \text{if} \quad \frac{P_{\text{atm}}}{P} \le C_r \\ \frac{C_2 C_f P}{\sqrt{T}} \left(\frac{P_{\text{atm}}}{P}\right)^{(1/\gamma)} \sqrt{1 - \left(\frac{P_{\text{atm}}}{P}\right)^{(\gamma-1)/\gamma}}, & \text{otherwise} \end{cases} \tag{5}$$

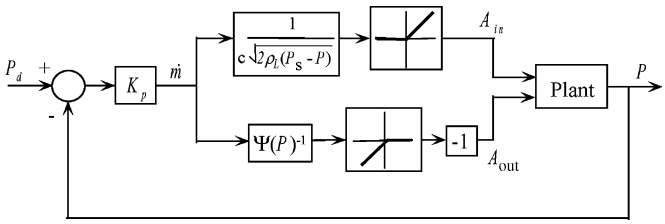

Fig. 8. Chamber pressure control loop.

chamber to be controlled. If the commanded force is positive, then the pressure in chamber A is actively controlled with no control effort directly acting on chamber B (i.e., chamber B remains closed). Conversely, for negative commanded forces, the pressure in chamber B is actively controlled with chamber A remaining closed. In the case of positive control effort (positive commanded force), the desired chamber pressure for chamber A is determined from (1) by

$$P_{\mathrm{A},d} = \frac{1}{A_{\mathrm{A}}}(F_d + P_{\mathrm{B}}A_{\mathrm{B}} + P_{\mathrm{atm}}A_r), \quad \text{for} \quad F_d \geq 0 \quad (8)$$

where $P_{\mathrm{A},d}$ is the desired pressure in chamber A and F_d is the desired actuator force. For the case of negative control effort, the desired chamber pressure for chamber B, also obtained from (1), is

$$P_{\mathrm{B},d} = \frac{1}{A_{\mathrm{B}}}(-F_d + P_{\mathrm{A}}A_{\mathrm{A}} - P_{\mathrm{atm}}A_r), \quad \text{for} \quad F_d < 0. \quad (9)$$

Once the desired chamber pressure is determined for a given direction of control effort, a pressure controller coordinates the exhaust valve and appropriate proportional fuel valve in order to realize the desired pressure. Fig. 8 shows the structure of the pressure control loop for a given actuator chamber. The error between the desired and the actual chamber pressure, multiplied by a proportional gain K_p, specifies a desired mass flow rate for each chamber as given by

$$\dot{m}_{\mathrm{A},d} = \begin{cases} K_p(P_{\mathrm{A},d} - P_{\mathrm{A}A}), & \text{for} \quad F_d \geq 0, \\ 0 & \text{otherwise}, \end{cases} \quad (10)$$

$$\dot{m}_{\mathrm{B},d} = \begin{cases} K_p(P_{\mathrm{B},d} - P_{\mathrm{B}}), & \text{for} \quad F_d < 0, \\ 0 & \text{otherwise}. \end{cases} \quad (11)$$

If the desired mass flow rate for a given chamber is positive, then the respective injection valve will actively control the flow of gas into the selected actuator chamber. Otherwise, the exhaust will be utilized to control the mass flow rate of the gas leaving the actuator chamber. The injection valve areas for chambers A and B are determined by

$$u_{\mathrm{in,A}} = A_{\mathrm{in,A}} = \begin{cases} \frac{\dot{m}_{\mathrm{A},d}}{c\sqrt{2\rho_{\mathrm{L}}(P_S - P_{\mathrm{A}})}}, & \text{for} \quad \dot{m}_{\mathrm{A},d} \geq 0, \\ 0 & \text{otherwise}, \end{cases} \quad (12)$$

$$u_{\mathrm{in,B}} = A_{\mathrm{in,B}} = \begin{cases} \frac{\dot{m}_{\mathrm{B},d}}{c\sqrt{2\rho_{\mathrm{L}}(P_S - P_{\mathrm{B}})}}, & \text{for} \quad \dot{m}_{\mathrm{B},d} \geq 0, \\ 0 & \text{otherwise}. \end{cases} \quad (13)$$

The conversion from mass flow rate to the orifice area is obtained from (3), where the actual mass flow should be a filtered version of the desired (i.e., the decomposition of hydrogen peroxide exhibits a first-order dynamics with a time constant of a few milliseconds). The exhaust orifice area obtained using (4) is specified by

$$u_{\mathrm{out}} = \begin{cases} A_{\mathrm{out,A}} = \frac{-\dot{m}_{\mathrm{A},d}}{\Psi(P_{\mathrm{A}})}, & \text{for} \quad \dot{m}_{\mathrm{A},d} < 0 \\ 0, & \text{for} \quad \dot{m}_{\mathrm{A},d}, \dot{m}_{\mathrm{B},d} \geq 0 \\ A_{\mathrm{out,B}} = \frac{-\dot{m}_{\mathrm{B},d}}{\Psi(P_{\mathrm{B}})}, & \text{for} \quad \dot{m}_{\mathrm{B},d} < 0. \end{cases} \quad (14)$$

Note that since the denominators of (12)–(14) are algebraic rather than dynamic functions, the controller behaves such that only one of the three valves is active at any given instant. Thus, the controller never simultaneously injects opposing chambers nor injects/exhausts a given chamber. Saturations of the valve commands are included to ensure that the injection valve area for a given chamber is positive for positive pressure error and zero otherwise, and that the exhaust valve area for a given chamber is positive for negative pressure error and zero otherwise. Using the pressure controller defined by (8)–(14) and the control parameters specified in Table I, the closed-loop system exhibits a force tracking bandwidth of approximately 4 Hz (i.e., as given by a -3-dB measure). This bandwidth is somewhat better than the system described in [1], and comparable to that described in [2] and [3].

TABLE I
PRESSURE CONTROLLER PARAMETERS

Parameter	Value
k	380 kJ/kg
T	505 K
ρ_L	1290 kg/m^3
c_p	1660 J/kg/K
γ	1.34
R	408 J/kg/K
c	0.13
C_f	0.29
C_r	0.54
K_p	0.35×10^{-8} kg/s/P

IV. ENERGETIC CHARACTERIZATION

Energetic characterization was conducted on a single degree-of-freedom arm, shown in Fig. 9, under closed-loop servo control. The previously described force controller was incorporated within an outer position control loop, which was used to determine the desired actuator force commanded to the PIDI controller. The outer loop consists of proportional-derivative control, with feedforward gravity compensation to cancel the static load of the 11.2 kg (25 lb) mass attached to the end of the arm.

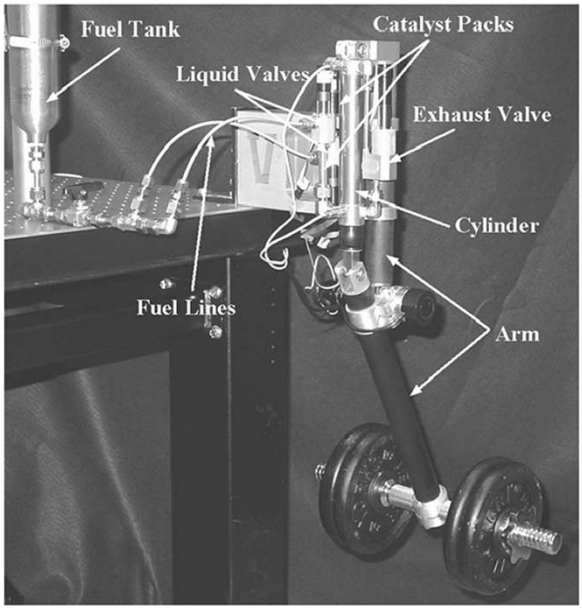

Fig. 9. Single-DOF arm with PIDI actuator.

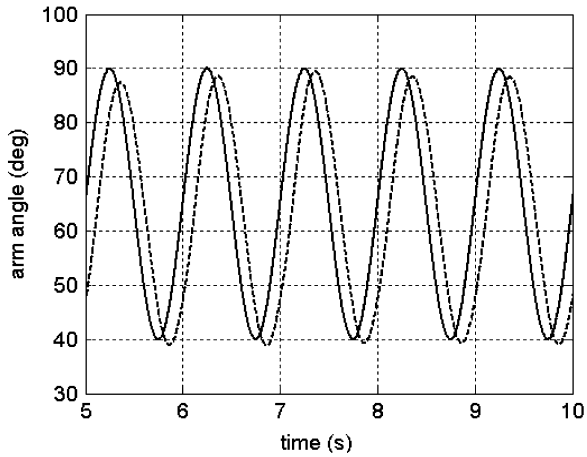

Fig. 10. Desired (solid) and actual (dashed) arm position for a 1-Hz command with an amplitude of 25°.

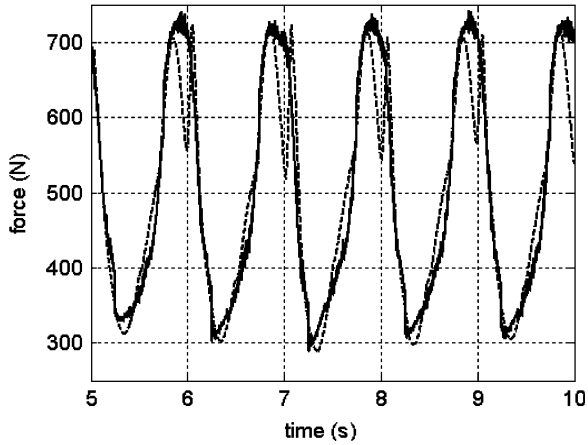

Fig. 11. Desired (solid) and actual (dashed) force of the PIDI actuator for 1-Hz motion tracking.

TABLE II
POSITION CONTROLLER PARAMETERS

Parameter	Value
m_a	11.6 kg
l_1	0.29 m
d_1	0.062 m
d_2	0.28 m
α	0.253 rad
$K_{p,arm}$	25 Nm/rad
$K_{d,arm}$	15 Nm·s/rad

The position (i.e., angle) of the arm is measured by an optical encoder (Renco model RHS15). The actuator torque specified by the outer loop is given by

$$\tau = K_{p,\mathrm{arm}}(\theta_d - \theta) + K_{d,\mathrm{arm}}(\dot{\theta}_d - \dot{\theta}) + m_a g l_1 \sin\theta_d \quad (15)$$

where $K_{p,\mathrm{arm}}$ is the proportional gain, $K_{d,\mathrm{arm}}$ is the differential gain, m_a is the mass of the arm load, g is the acceleration due to gravity, l_1 is the length of the forearm, θ is the actual arm angle, and θ_d is the desired arm angle. The desired torque is then transformed to a desired force via the inverse of the Jacobian as follows:

$$F_d = \left(\frac{\sqrt{d_1^2 + d_2^2 - 2d_1 d_2 \cos(\theta + \alpha)}}{d_1 d_2 \sin(\theta + \alpha)} \right) \tau \quad (16)$$

where d_1, d_2, and α are geometric parameters that describe the kinematic relationships of the actuator/arm linkage (see [1] for more geometric and kinematic details). Figs. 10 and 11 show the experimental results (i.e., the position tracking results and the corresponding force tracking) for tracking a 1-Hz position command at an amplitude of 25° by using the outer-loop controller defined by (15) and (16) and the controller parameters of Table II. Note that the actuator force was measured indirectly by measuring the pressure in each cylinder with the previously mentioned pressure sensors. PIDI pressure control results in the force tracking shown in Fig. 11, which in turn yields the desired 1-Hz motion tracking shown in Fig. 10. Recall that the desired force trajectory shown in Fig. 11 was generated by the outer position control loop. The "ripple" in the actuator force in Fig. 11 occurs when the active cylinder chamber is at its minimum volume, which maximizes the sensitivity of the pressure to the exhaust valve command. This is a nonlinear effect that is best accommodated by a nonlinear controller. Despite this, the amount of torque ripple exhibited by the actuator is fully filtered from the system by the inertial dynamics of the arm, and thus the net effect on the arm motion is negligible. Figs. 12 and 13 show the results for tracking a square wave at a frequency of 0.25 Hz and an amplitude of 15°.

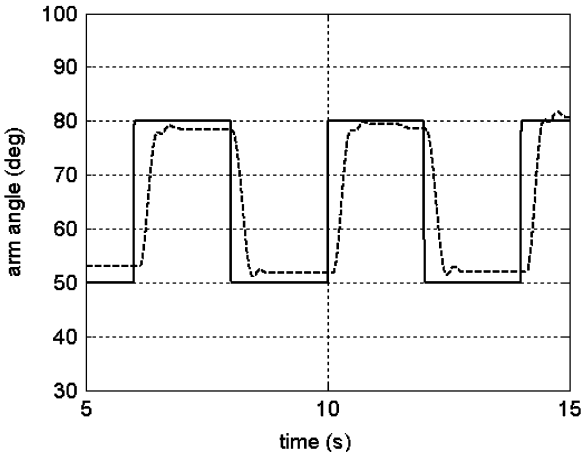

Fig. 12. Desired (solid) and actual (dashed) arm position for 0.25-Hz square wave command.

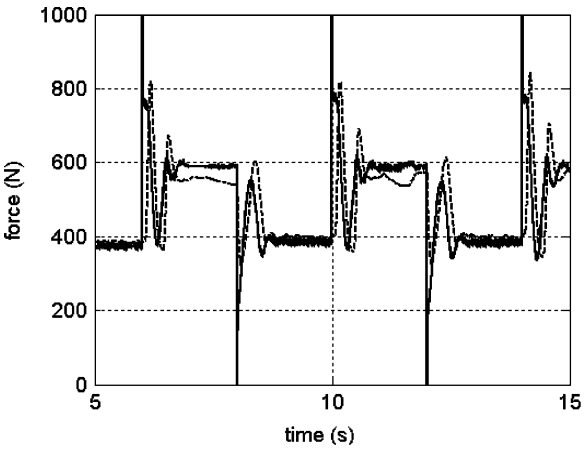

Fig. 13. Desired (solid) and actual (dashed) force of the PIDI actuator for 0.25-Hz square wave motion.

The average steady-state error in the step response is approximately 2°. Recall that the desired force trajectory shown in Fig. 13 was generated by the outer position control loop.

In order to quantify the energetic performance of the monopropellant-powered actuator, a figure of merit is required. This paper utilizes the actuation potential, a figure of merit proposed in [1], which is the product of the energy density of the fuel source, the efficiency of conversion from the power source to controlled mechanical energy in the joint space, and the power density of the actuator. The actuation potential is given by

$$A_p = e_s \eta p_a \tag{17}$$

where e_s is the energy density of the monopropellant, η is the conversion efficiency of the system, and p_a is the power density of the actuator. The monopropellant used throughout this work is 70% hydrogen peroxide (30% water by weight), with an adiabatic decomposition temperature of 232 °C (450 °F) and a lower heating value of 400 kJ/kg. The energy density of the monopropellant has been previously measured (see, for example, [11]), and thus characterization of the actuation potential requires measurement of the conversion efficiency (from stored chemical energy to controlled mechanical work) and the power density of the actuator. The conversion efficiency will, in general, depend upon the characteristics of the actuator motion and the load imposed on the actuator. Since the actuators of a human-scale robot are typically engaged in the motion control of inertial loads within a conservative force field (e.g., limb segments in the presence of gravity), a representative energetic characterization should reflect these conditions. As such, the efficiency of energy conversion for the proposed system was characterized via the closed-loop sinusoidal position tracking of an 11.2 kg (25 lb) inertial endpoint in a vertical plane (i.e., lifting a weight through a gravitational field) at a frequency of 1 Hz. The efficiency of conversion was measured by measuring the average rectified mechanical power output over an integer number of motion cycles, measuring the fuel flow rate over the same period,and using knowledge of the lower heating value to compute the efficiency.

A. Conversion Efficiency

Experiments were conducted to measure the actual efficiency in converting the energy stored in the 70% concentration hydrogen peroxide to controlled mechanical work. The arm was commanded to track a sinusoidal motion trajectory, and the controlled mechanical power output was measured via the combination of pressure sensors and a joint angle encoder (which together enabled computation of the joint torque imposed by the actuator) and a joint angle tachometer (Servo-Tek SA-740B-1, which was used to measure the joint angular velocity). The instantaneous power was calculated by

$$\mathrm{P}(t) = |\tau \dot{\theta}| \tag{18}$$

where τ is the delivered torque, $\dot{\theta}$ is the angular velocity of the arm, and the absolute-value operator reflects the fact that the system is assumed energetically nonconservative. The average power was calculated by integrating over an integer number of cycles as

$$P_{\mathrm{avg}} = \frac{\int_{t_1}^{t_2} P(t)dt}{t_2 - t_1}. \tag{19}$$

The mass of monopropellant consumed during the time from t_1 to t_2 was indirectly determined by measuring the initial mass of the fuel in the (nitrogen charged) blowdown tank, recording the pressure of the nitrogen gas in the blowdown tank, assuming an isothermal process inside the constant-volume tank, and calculating the volume occupied by the nitrogen from the ideal gas equation, which in turn yields the volume of propellant remaining in the tank. Since the volume and density of the liquid propellant are known, the mass of remaining propellant is easily calculated. The conversion efficiency based upon the lower heating value was then calculated by

$$\eta = \frac{P_{\mathrm{avg}}(t_2 - t_1)}{\hat{e}_s m_{\mathrm{H_2O_2}}} \tag{20}$$

where $\hat{e}_s$ is the lower heating value of 70% hydrogen peroxide (0.4 MJ/kg as given by [11]) and $m_{\mathrm{H_2O_2}}$ is the mass of fuel

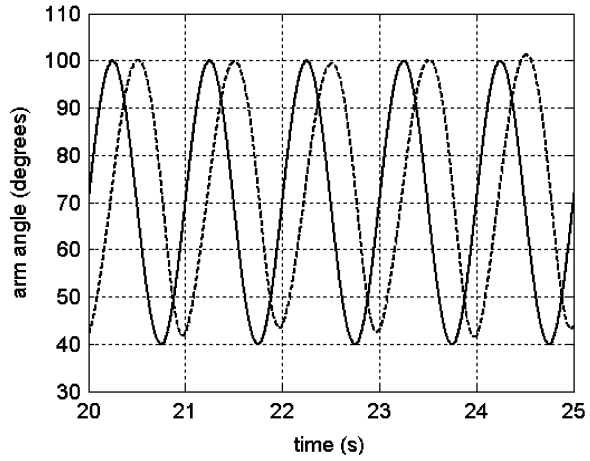

Fig. 14. Desired (solid) and actual (dashed) 1-Hz arm motion for the characterization of conversion efficiency of the PIDI actuator.

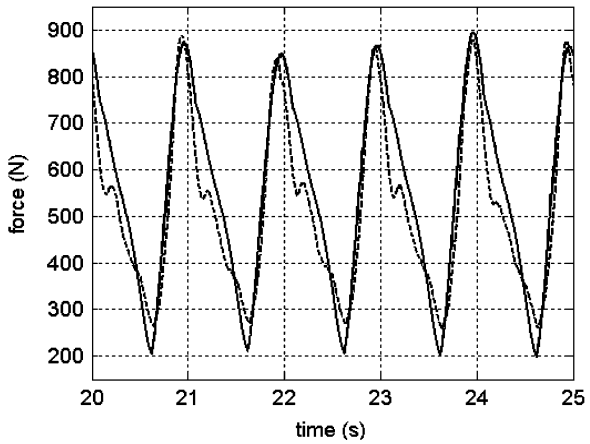

Fig. 15. Desired (solid) and actual (dashed) force corresponding to the 1-Hz arm motion for characterizing the conversion efficiency of the PIDI actuator.

consumed during the time duration of t_1 to t_2 (as derived from the measured change in volume and known density).

The energetic conversion efficiency depends strongly upon the corrective action of the outer position control loop. An inverse relationship exists between the conversion efficiency and the achievable closed-loop tracking bandwidth of the actuator. The outer-loop control gains were therefore adjusted for improved energetic efficiency at the cost of sacrificing tracking performance. Figs. 14 and 15 show the arm position tracking and corresponding actuator force tracking for a 1-Hz motion command with an amplitude of 30° by using outer loop control gains of $K_{p,\mathrm{arm}} = 18\,\mathrm{N}\cdot\mathrm{m/rad}$ and $K_{d,\mathrm{arm}} = 5\,\mathrm{N.m.s/rad}$. Note that these gains limit the achievable tracking bandwidth, as evidenced by the increased phase lag shown in Fig. 15 relative to the tracking results of Fig. 10, but still enable good 1-Hz motion tracking. Several tests were conducted for the 1-Hz motion command, each measured over a span of 30 s, and the efficiency was computed using (20). Based on several trials, the average energy efficiency of conversion was found to be $\eta = 45\%$.

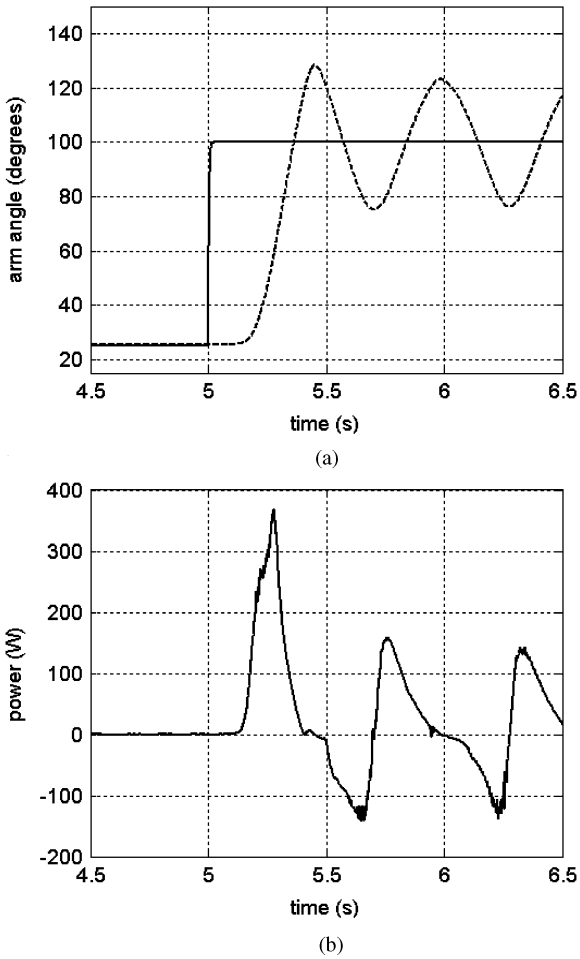

Fig. 16. Experimental measure of maximum deliverable power. (a) Step response. (b) Measured output power.

B. Power Density

The mass-specific power density of the actuator was found by measuring the maximum deliverable output power and normalizing by the measured mass of the actuator. For the limited displacement cylinder, the maximum deliverable power was measured using a series of step responses. Fig. 16 shows the step response and output power for one such step response. The step response was measured for outer-loop control gains chosen to deliver the fastest achievable rise time with no consideration of settling time (i.e., actuator power density is an open-loop characteristic and was thus measured without regard to closed-loop behavior). The tests were conducted for several actuator loads, and the maximum deliverable power was found to be 365 W for an endpoint mass of 7 kg. The total mass of the PIDI actuator shown in Fig. 6 is 0.95 kg, and thus the resulting mass-specific power density of the actuator is $p_a = 384$ W/kg.

C. Actuation Potential

The lower heating value of 70% hydrogen peroxide is $\hat{e}_s = 0.4$ MJ/kg. Because of the propellant storage in a blowdown tank, the energy density of the fuel is effectively reduced by the

additional weight of the fuel tank, as given by

$$e_s = \frac{m_{\text{fuel}}\hat{e}_s}{m_{\text{fuel}} + m_{\text{tank}}} \tag{21}$$

where m_{fuel} is the total mass of fuel in the tank and m_{tank} is the mass of the tank. A reasonable estimate of the energy density is obtained assuming a 10-L composite blowdown tank with a mass of approximately 2 kg (see, for example, [12]). Since the density of 70% hydrogen peroxide is 1.3 kg/L, a 10-L composite tank with a mass of 2 kg would reduce the effective mass-specific energy density of the fuel $\hat{e}_s$ from 0.4 to 0.35 MJ/kg. Using this energy density along with the measured efficiency of conversion $(\eta = 45\%)$ and power density ($p_a = 384$ W/kg), the actuation potential for the PIDI actuator, computed using (17), is $A_p = 60.5$ kJ $\cdot$ kW/kg^2. The actuation potential of a neodymium-based servomotor actuator with a harmonic drive gearhead, powered by nickel–zinc batteries was found in [1] to be approximately $A_p = 4.8$ kJ $\cdot$ kW/kg^2. Thus, the proposed direct-injection monopropellant-powered actuator provides an actuation potential more than an order of magnitude (i.e., 12.6 times) higher than a state-of-the-art battery/servomotor system. Further, the actuation potential for the PIDI actuator provides a factor of improvement of 3.7 relative to that of the centralized prototype presented in [1] and of 1.2 relative to the SIDI prototype detailed in [2] and [3].

V. Conclusion

This paper presented the design and energetic characterization of a PIDI monopropellant-powered actuator. The paper presented the design of the proportional-injection fuel valve, a controller for closed-loop actuator force control, and the experimental characterization of the energetic behavior of a prototype actuator. The described monopropellant system provides more than an order of magnitude improvement in the energetic figure of merit relative to the state-of-the-art battery/servomotor combination and a 20% improvement relative to a previously presented solenoid-injected monopropellant-powered actuator prototype.

References

[1] M. Goldfarb, E. J. Barth, M. A. Gogola, and J. A. Wehrmeyer, "Design and energetic characterization of a liquid-propellant-powered actuator for self-powered robots," *IEEE/ASME Trans. Mech.*, vol. 8, no. 2, pp. 254–262, Jun. 2003.

[2] B. Shields, K. F. Fite, and M. Goldfarb, "Control of a direct injection liquid fueled actuator," presented at the *ASME Int. Mech. Eng. Congr. and Exposition*, 2004, IMECE2004-59442.

[3] B. Shields and M. Goldfarb, "Design and energetic characterization of a solenoid injected liquid monopropellant powered actuator for self-powered robots," in *Proc. IEEE Int. Conf. Robotics Automation*, 2005, pp. 242–247.

[4] H. C. Hearn, "Flight performance of a high-impulse monopropellant thruster," *J. Thermal Analy. Calorimetry*, vol. 59, pp. 901–911, 2000.

[5] D. C. Morrisey, "Historical perspective. Viking mars lander propulsion," *J. Propulsion Power*, vol. 8, no. 2, pp. 320–331, 1992.

[6] D. L. Hitt, C. M. Zakrzwski, and M. A. Thomas, "MEMS-based satellite mircopropulsion via catalyzed hydrogen peroxide decomposition," *Smart Mater. Struct.*, vol. 10, no. 6, pp. 1163–1175, 2001.

[7] T. G. McGee, J. W. Raade, and H. Kazerooni, "Monopropellant-driven free piston hydraulic pump for mobile robotic systems," *ASME J. Dynamic Syst., Measur. Control*, vol. 126, no. 1, pp. 75–81, 2004.

[8] K. Fite, J. Mitchell, M. Goldfarb, and E. J. Barth, "Design and characterization of a high-bandwidth rotary hot gas valve," presented at the *ASME Int. Mech. Eng. Congr. and Exposition*, 2004, IMECE2003-42746.

[9] K. B. Fite, J. Mitchell, E. J. Barth, and M. Goldfarb, "Sliding mode control of a direct-injection monopropellant-powered arm," in *Proc. Amer. Control Conf.*, 2004, pp. 4461–4466.

[10] K. A. Al-Dakkan, E. J. Barth, and M. Goldfarb, "A multi-objective sliding mode approach for the energy saving control of pneumatic servo systems," presented at the *ASME Int. Mech. Eng. Congr. and Exposition*, 2003, IMECE2003-42746.

[11] L. H. Dierdorff *et al.*, *Hydrogen Peroxide Physical Properties Data Book*. 2nd ed. Buffalo, NY: Becco Chem. Div. FMC Corp., 1954.

[12] W. H. Tam, I. A. Ballinger, J. Kuo, W. D. Lay, S. F. McCleskey, P. Morales, Z. R. Taylor, and S. J. Epstein, "Design and manufacture of a composite overwrapped xenon conical pressure vessel," presented at the *AIAA/ASME/SAE/ASEE Joint Propulsion Conf.*, 1996, AIAA 96-2725.

Kevin B. Fite (S'99–A'02–M'03) received the B.E., M.S., and Ph.D. degrees from Vanderbilt University, Nashville, TN, in 1997, 1999, and 2002, respectively, all in mechanical engineering.

He is currently a Research Associate in the Department of Mechanical Engineering, Vanderbilt University. His research interests include power-autonomous robot actuation, the design and control of electromechanical and fluid power systems, and the design and control of upper- and lower-extremity prostheses.

Michael Goldfarb (S'93–M'95) received the B.S. degree from the University of Arizona, Tucson, in 1988, and the S.M. and Ph.D. degrees from the Massachusetts Institute of Technology, Cambridge, in 1992 and 1994, respectively, all in mechanical engineering.

In 1994, he joined the Department of Mechanical Engineering, Vanderbilt University, where he is currently a Professor. His current research interests include the design of high-energy-density robotic actuators, the control of fluid-powered actuators, and the design and control of haptic interfaces and telemanipulator systems.